Dynamics of a CO_2 laser with delayed feedback: The short-delay regime

F. T. Arecchi,* G. Giacomelli, A. Lapucci, and R. Meucci
Istituto Nazionale di Ottica, Largo Fermi 6, Firenze, Italy
(Received 6 August 1990; revised manuscript received 4 October 1990)

We present an experimental and theoretical study of the dynamics of a CO_2 laser with delayed feedback. Working with a delay time such that its product with the bandwidth of the feedback loop yields a number close to unity (so-called short-delay regime), we show evidence of a low-dimensional chaos, reached by the destabilization of a two-dimensional torus (Curry-Yorke route to chaos). A suitable model provides numerical solutions in agreement with the experiment. We discuss under which conditions our system reduces to an Ikeda-type delayed dynamics.

I. INTRODUCTION

In the past years, the onset of low-dimensional chaotic dynamics has been extensively explored in a large variety of physical systems. The minimal condition for the onset of a chaotic dynamics ("minimal chaos") is the presence of at least three degrees of freedom (DOF) as shown, e.g., by the Lorenz equations.[1]

In the physics of single-mode lasers three relevant variables are actually present whenever the time scales of field, polarization, and population inversion are of the same order, and indeed the corresponding Maxwell-Bloch equations are isomorphic to the Lorenz equations.[2] However, in most cases of physical interest there are large differences among the damping times of the three lasers' variables. This suggests a classification into class-A, -B, and -C lasers,[3] ruled, respectively, by one, two, and three dynamical equations. In the case of a class-B laser, minimal chaos has been observed in a variety of configurations implying the addition of a third degree of freedom. This third DOF can be added for instance by a feedback loop acting on a time scale comparable with that of the other two internal DOF's. Such a situation was explored in a series of recent papers.[4] On the other hand, introduction of a delay in a nonlinear dynamical system is generally reputed to be a source of a high-dimensional chaos.[5] From a theoretical point of view dissipative systems ruled by delayed feedback are generally modeled by delayed differential equations of the kind

$$\dot{\mathbf{X}}(t)=\mathbf{F}(\mathbf{X}(t),\mathbf{X}(t-\tau)) \tag{1}$$

where $\mathbf{X}$ is a vector field and $\mathbf{F}$ is a nonlinear term including dissipative effects. The presence of delay relates the dynamical variable to a continuous set of initial conditions, thus the solutions of problem (1) should be found in an infinite-dimensional phase space. Mallet-Paret[6] instead demonstrated that the effective topological dimension of the attractor of such systems is finite. Apart from the general theorem of Ref. 6 no general consensus is available on a sound evaluation of the relevant number of DOF's in a delayed system. In this paper we study both experimentally and theoretically the behavior of a single-mode class-B laser with a delayed intensity feedback, exploring situations where the delay is short enough to confine the dynamics near minimal chaos. In a planned companion paper,[7] we explore the opposite limit of a very long delay which provides a large number of DOF's and hence a high-dimensional chaos. In Sec. II we describe the physical system, display the model equations, and discuss the conditions under which our system reduces to the Ikeda case. Section III describes the experimental setup. Section IV analyzes the experimental data. Finally in Sec. V data are compared with a numerical solution of the model. A preliminary report of this work has been presented at a recent conference.[8]

II. THE CLASS-B DELAYED FEEDBACK LASER

Let us consider a single-mode class-B laser and call x the intensity, y the population inversion, and z the voltage signal provided by a photodetector looking at the laser output and applied via a filter of bandwidth β and a delay of duration τ to an intracavity electro-optic modulator. The corresponding equations with a suitable scaling of the variables discussed elsewhere[3,4] are

$$\begin{aligned}
&\frac{\dot{x}}{k}+x=xy-\alpha x\sin^2 z_d\ ,\\
&\frac{\dot{y}}{\gamma}+y=-xy+A\ ,\\
&\frac{\dot{z}}{\beta}+z=B-rx\ ,
\end{aligned} \tag{2}$$

where k and γ are the cavity and population decay rate, β is the bandwidth of the feedback loop, A is the normalized pump ($A=1$ at threshold), and α represents the strength of coupling via the loss modulator, which in first approximation is a sine squared function of the delayed feedback voltage $z_d=z(t-\tau)$.

The crucial question now is the following: how many DOF's are effective in Eq. (1)? As shown in Ref. 4, for $\tau=0$ (no delay) the feedback system already provides a minimal chaos.

For a generic τ, the Shannon theorem[9] provides a simple powerful argument to evaluate the number of DOF's added by delay in the feedback loop. Indeed, to solve this problem we have to specify the set of initial conditions on

the interval $[-\tau,0]$. Such a set can be described using a Fourier series with harmonics of the fundamental frequency $\nu=1/\tau$, each one counting for two DOF's. Because of the filtering through the finite bandwidth β of the feedback loop, only a limited number of those frequencies is effective on the dynamics. Precisely, the number of additional initial conditions to be accounted for in the open interval $(-\tau,0)$ is given by the product $N=2\beta\tau$.

A recent conjecture[10,11] was developed from this basic idea in order to evaluate the dimensions of the attractors for delay systems belonging to the class explored over the past years by Ikeda and co-workers as well as by other groups.[12] These systems are based on the following model equation:

$$\frac{\dot{x}}{\beta}+x=f(x_d) \tag{3}$$

where $x_d=x(t-\tau)$ is the delayed variable. The fact that our system is not reducible to Eq. (3) in a straightforward way is shown, for instance, by our route to chaos, which is Curry-Yorke' (CY), as shown in the forthcoming sections, whereas Eq. (3) becomes chaotic according to the Ruelle-Takens-Newhouse[13] (RTN) model, as shown in Ref. 14.

The main difference between these two scenarios is related to the fact that in the RTN model a three-dimensional torus is transformed into a strange attractor whereas in the CY model chaos appears directly after the onset of two frequencies, as a destabilization of a two-dimensional torus.

To appreciate the difference between the two groups of equations we consider the following limit circumstance. Keeping a fixed $\beta\tau$, let $\beta\to 0$, $\tau\to\infty$, that is, introduce a large delay and a strong filter. The contributions $2\beta\tau$ to the number of DOF's remain constant. However, on long-time scales the laser dynamics can be adiabatically eliminated and thus the laser is reduced to a simple light source serving as input to the modulator. Indeed, if the delay time τ is much longer than the longest characteristic time of a class-B laser which is of the order of $1/\gamma$,[3] we can solve at equilibrium the first two Eqs. (2) for x and y and substitute the solution $x=f(z)$ into the third one which reduces to

$$\frac{\dot{z}}{\beta}+z=B-rf(z_d)\ . \tag{4}$$

Thus our problem becomes equivalent to Eq. (3) for delay $\tau\gg 1/\gamma$. The above asymptotic argument has been offered for the sake of comparing our and Ikeda's systems. A more rigorous treatment would require a detailed comparison of decay times and a center manifold analysis as developed already for nondelayed lasers.[15] However, the extension of that technique to delayed systems has unresolved difficulties, and it is anyway beyond the scope of this paper.

The formal solution of Ikeda Eq. (3)

$$x(t)=\beta\int_0^t e^{-\beta(t-u)}f(x(t-u-\tau))du \tag{5}$$

suggested the following conjecture: "the dimension of a chaotic attractor of system (3) is given by τ/τ_c, where τ_c is the correlation time of the driving force $f(x)$".[10,11] This conjecture, verified experimentally in an optical bistable hybrid system,[11] would be difficult to apply in our case. Indeed assignment of a correlation time for a nonlinear driving force in our complex dynamics would be an *a posteriori* characterization, as in fact done in Ref. 11.

We discuss in a planned paper[16] the possibility to calculate at least the dimension of the phase space within which the motion is embedded.

III. EXPERIMENTAL SETUP

The system without delay has been described in detail in Ref. 4. The experimental setup is shown in Fig. 1. We employ a single-mode homogeneously broadened CO_2 laser with an intracavity electro-optic modulator controlling the cavity losses.

The feedback loop consists of a wide band high voltage amplifier coupling the intensity signal from the fast Hg-Cd-Te detector to the modulator. The delay of 4.7 μs is inserted in the feedback loop by using an analog delay line after the first amplification stage. As control parameters we use the bias voltage applied to the amplifier preceding the electro-optic modulator and the feedback loop gain, keeping the pump parameter constant.

From an experimental point of view the only accessible variables are the laser intensity and the feedback voltage. We acquire the intensity signal by a fast 12-bit analog-to-digital-(AD) converter (LeCroy 6810) with a minimum sampling time of 200 nsec. Such a system permits recording of long-time series (up to 512 K samples) with a high time and amplitude resolution. We also perform an analog filtering of the signal before acquisition using an

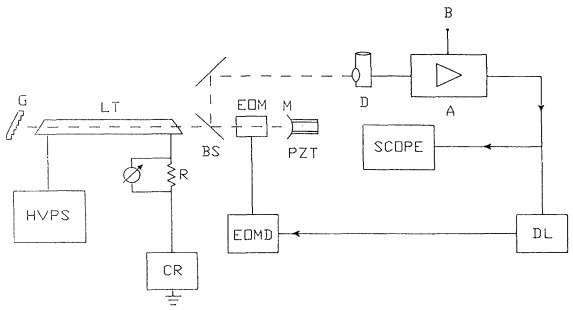

FIG. 1. Outline of the experimental setup. G is a 100 1/mm grating. LT is the CO_2 laser tube water cooled and excited by means of a high-voltage power supply (HVPS) with current regulation (CR). R is a precision resistor to measure the discharge current. EOM is a CdTe electro-optic modulator with a half wavelength voltage $V_{\lambda/2}=4240$ V. The total reflection mirror M is mounted on a piezo-translator (PZT). D is a fast Hg-Cd-Te (liquid N_2 cooled detector). A is the first amplification stage of the feedback loop, and B is the bias voltage. DL is the 4.7-μs delay line. EOMD is the electro-optic modulator driver.

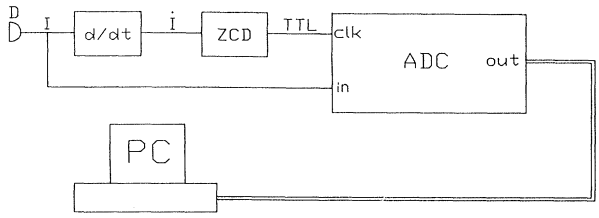

FIG. 2. Block diagram of the acquisition system used for a hardware reconstruction of the Poincaré section. The signal I from the photodetector D is digitized by an eight-bit analog-to-digital converter (ADC). The acquisition is syncronized by the zero cross detection (ZCD) on the time derivative of the signal I. The link between ADC and the personal computer (PC) is realized via the GPIB IEEE-488 interface.

eight-pole Rockland high-pass filter, with the aim of isolating different features of chaotic attractors. In order to characterize accurately the different behaviors we have based our observations on various indicators: time sequences, power spectra, phase-space portraits, autocorrelation functions, correlation dimensions, and Poincaré sections. The corresponding evaluations are done off line via software after the digital acquisition of the intensity signal. However, we have also implemented a hardware reconstruction of Poincaré sections in order to allow the scanning of one of the two control parameters. In Fig. 2 a block diagram of this setup is reported. Both in the software and in the hardware reconstructions we have built the Poincaré maps plotting the amplitude of the intensity signal at the local maximum versus the previous one. In the hardware case the maximum condition is realized by a zero crossing detection of the derivative of the intensity signal and the AD conversion is triggered by this event.

IV. ANALYSIS OF EXPERIMENTAL DATA

Our data show clear evidence of a Curry-Yorke transition to chaos. Keeping the gain constant we have collected different sets of data at increasing B, observing two

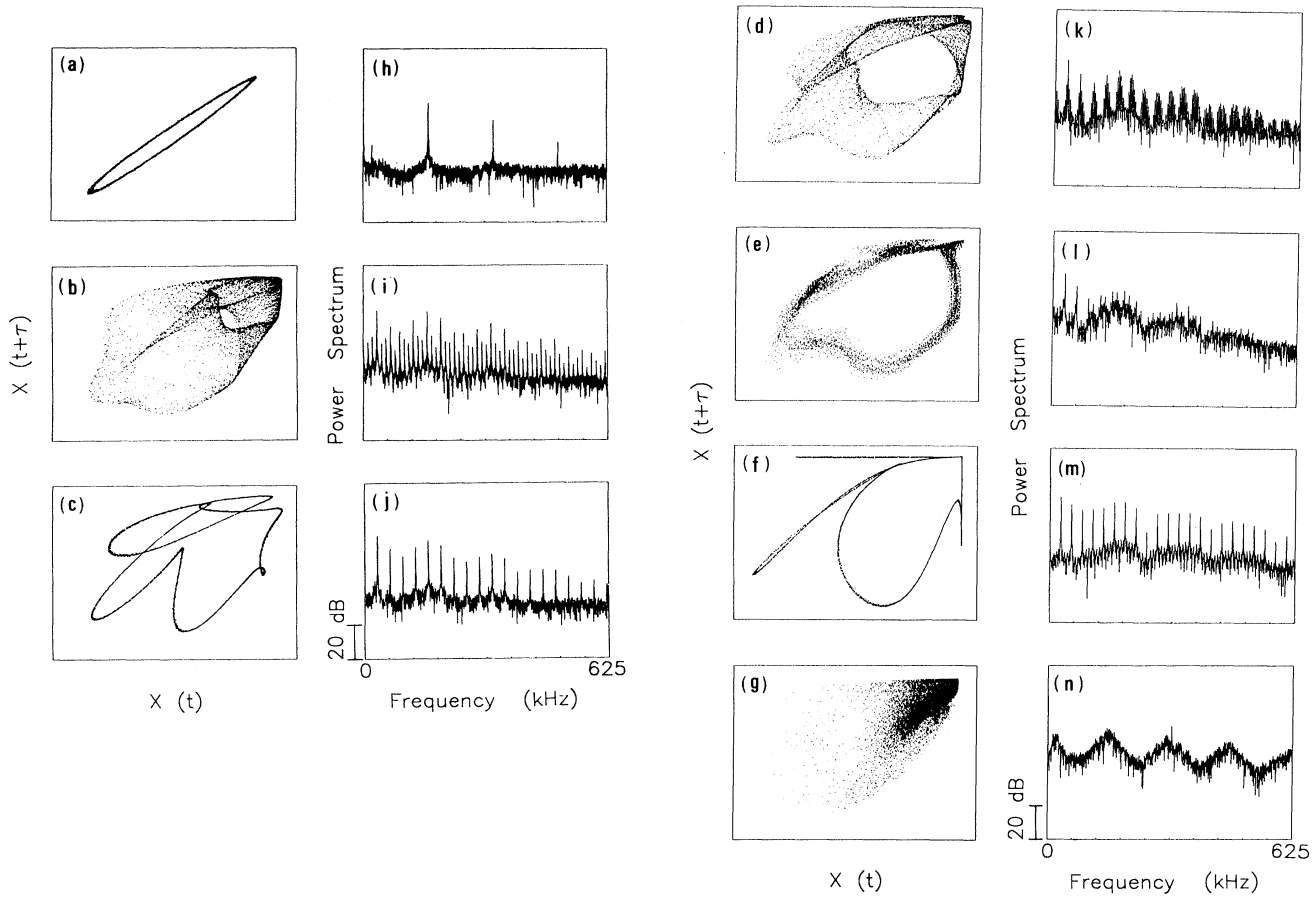

FIG. 3. Phase-space portraits, $x(t)$ vs $x(t+\tau)$ where τ is the delay time, and corresponding power spectra obtained by increasing the bias voltage B for a fixed value of r and for a pump $A=2.05$; the winding number w is also reported for toroidal and locked motions. (a) $B=542$ V; (b) $B=620$ V, $w=4.6$; (c) $B=645$ V, $w=5$; (d) $B=660$ V, $w=5.1$; (e) $B=670$ V; (f) $B=690$ V, $w=6$; (g) $B=785$ V.

Hopf bifurcations as reported in Fig. 3. In that figure we present power spectra and phase portraits. The phase portraits have been realized by an embedding technique, that is, we have plotted x_n versus x_{n+N}, where $N\Delta t$ is roughly equal to the delay time τ, Δt being the sampling time. The associated power spectra are obtained by a fast Fourier transform (FFT) algorithm using 16 384 points. Figure 3(a) shows a limit cycle born from the destabilization of a stationary solution (fixed point, not reported here). Another bifurcation gives rise to a second incommensurate frequency generating a motion on a torus ["torus 1", Fig. 3(b)]. Actually between these two behaviors there is a small window of parameters in which the two frequencies are locked (we label this behavior that will be evident in Figs. 4 and 5 as "lock 0"). Increasing B yields successively a small locking region ["lock 1" in Fig. 3(c)] and a second torus ["torus 2," Fig. 3(d)]. A further increase of B leads to the destabilization of the torus into a chaotic motion ["chaos 1," Fig. 3(e)]. This is followed by a wide window corresponding to a stable locked motion ["lock 2," Fig. 3(f)] ending in a fully developed chaotic behavior ["chaos 2," Fig. 3(g)]. This eventually collapses back into a new torus and limit cycle.

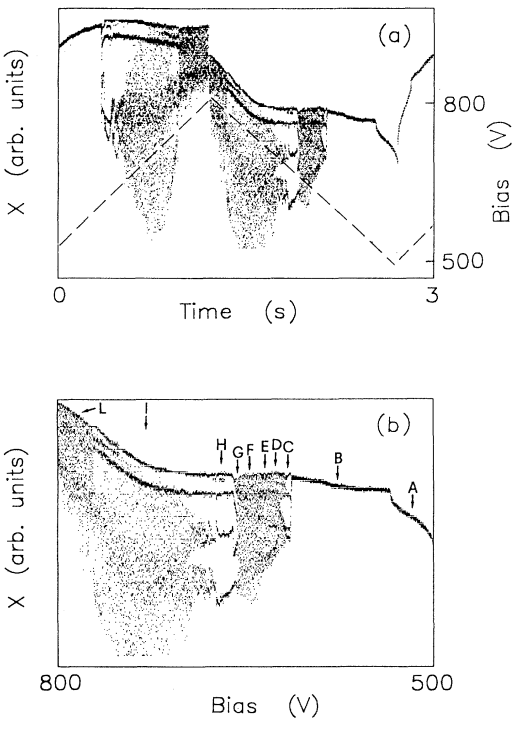

FIG. 4. (a) Bifurcation diagram obtained by using the measurement scheme reported in Fig. 2 and scanning the bias voltage with a triangular wave with a period of 3s (dashed line). (b) Downwards scanning with identification of the various dynamical regimes: A, limit cycle 1; B, limit cycle 2; C, lock 0; D, torus 1; E, lock 1; F, torus 2; G, chaos 1; H, lock 2; I, chaos 2; L, torus 3.

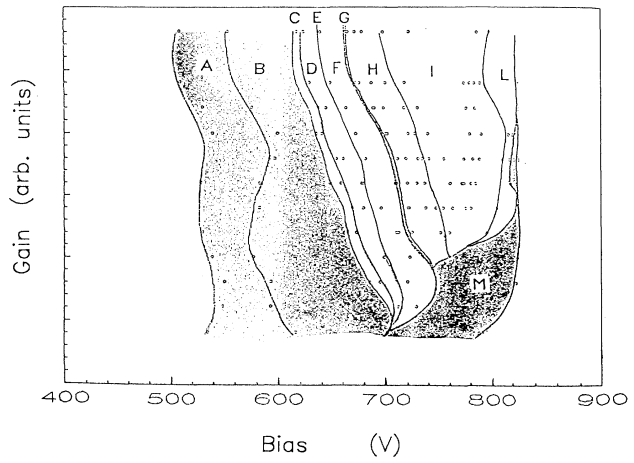

FIG. 5. Parameter space representation B(bias)-r(gain) at a fixed pump $A=2.05$ (downwards scanning). Letters $A-L$ have the same meaning as in Fig. 4. M represents the limit cycle 3 present for low gains.

Figure 4 reports a bifurcation diagram obtained implementing Poincaré sections as described in Sec. II and scanning with a triangular wave the bias at a fixed gain. First of all we can observe a hysteresis pointed out by the different size and location of the dynamical windows in the up and down scanning of B [see triangular wave in the lower part of Fig. 4(a)]. The arrows show the positions of the behaviors reported in Fig. 3. Figure 5 is a parameter space B-r representation of the different dynamical domains corresponding to a downwards scan.

In Fig. 6 we compare the motion at the onset of chaos and when the chaotic motion is fully developed. For this purpose we report the temporal behavior, the autocorrelation, and the fractal dimension of the signal. The autocorrelation function is defined as

$$C(\tau)=\frac{\langle x(t)x(t-\tau)\rangle-\langle x\rangle^2}{\langle x^2\rangle-\langle x\rangle^2}\ , \tag{6}$$

where $\langle\ \rangle$ denotes time average.

The fractal dimension D_2 is evaluated calculating the slope of the log-log plot of the correlation integral by means of the Grassberger-Procaccia method.[17] The first row [Fig. 6(a)] shows the above-mentioned indicators relative to a motion on a torus; the second row [Fig. 6(b)] is relative to the motion at the onset of chaos, corresponding to the behavior reported in Fig. 3(d).

Figure 6(c) refers to the same signal when it has been analogically high-pass filtered before acquisition. Finally Fig. 6(d) shows the indicators for the fully chaotic behavior previously shown in Fig. 3(g).

It is interesting to stress that the correlation dimension plots in Fig. 6(b) clearly show the existence of a saturation plateau at a value $D_2\simeq 1$ for larger correlation distances, but also suggest the presence of a higher dimension for shorter correlation distances, which cannot be well recognized because of the small number of bits on

which the chaotic high-frequency motion is recorded. For this reason we have filtered out the low-frequency part of the signal so that it has been possible to obtain a much better resolution on the high-frequency motion. In this case [Fig. 6(c)] we can clearly recognize a saturation plateau in the correlation dimension measurements at a value $D_2 \simeq 3.3$ which might be affected by the filtering process.[18]

One should notice that even in the fully developed chaos with $D_2 \simeq 3.3$ the laser intensity has still a correlation time T_c of about 140 μs which is much longer than the delay time $\tau = 4.7$ μs. We might be tempted to apply the conjecture by Le Berre *et al.*[11] and correlate the dimension of the chaotic attractor with the ratio τ/T_c. This ratio, however, is here $\tau/T_c \simeq 0.033$. In fact, that conjecture refers to an equation such as Eq. (4) and requires the correlation time of the driving force on the right-hand side of Eq. (4). As shown in Sec. II, only asymptotically can we reduce our dynamics to such a form, and the correlation function of the intensity here measured is by no means the correlation function of the overall driving force implied by Eq. (4).

Figure 7 is a detailed sequence which illustrates the torus breaking, showing evidence of the Curry-Yorke transition. Here we have reported the Poincaré sections and the associated fractal dimensions (i.e., measured on the Poincaré section data files). The four different plots correspond to increasing values of the control parameter within the transition interval between the torus and the first chaotic behavior.

The first of these plots shows that the torus motion corresponds to a cycle in the Poincaré section and the dimension calculation and yields a saturation plateau at a value 1 in the slope of the correlation integral. When the torus breaks, the cycle shows "wrinkles" and the Grassberger-Procaccia algorithm does not provide a plateau of constant slope in the correlation integral for different correlation distances. Finally when the torus is

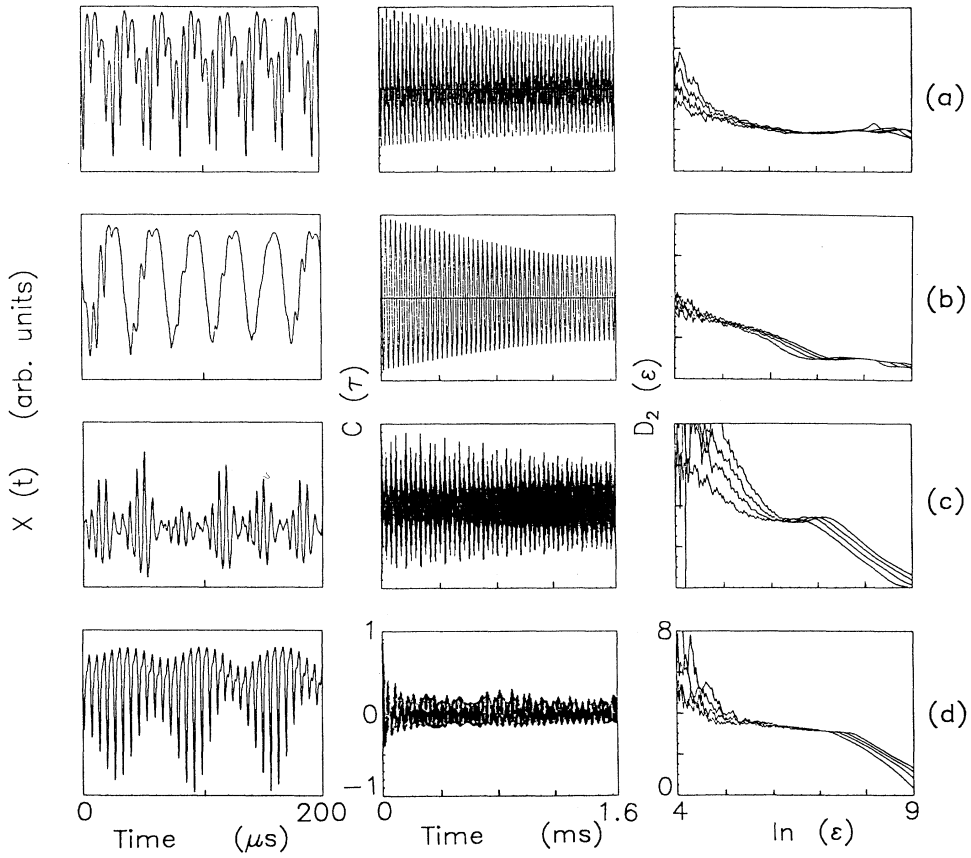

FIG. 6. Left column: temporal evolution of the laser intensity $x(t)$. Central column: autocorrelation function $C(\tau)$ of the laser intensity. Right column: Correlation integral slopes vs $\ln(\varepsilon)$, calculated by means of the Grassberger-Procaccia algorithm using embedding dimensions 8-10-12-14, embedding delay 4, around 15 points per quasicycle and a total number of points N_p different from one time sequence to the other. The figures correspond to the following regimes: (a) torus 2 ($N_p = 20\,000$, $D_2 = 1.95 \pm 0.05$); (b) chaos 1 ($N_p = 30\,000$, $D_2 = 1.02 \pm 0.02$ growing towards 2.9 for low ε); (c) high-pass filtered signal of chaos 1 ($N_p = 30\,000$, $D_2 = 3.27 \pm 0.02$); (d) fully developed chaos (chaos 2) ($N_p = 50\,000$, $D_2 = 3.29 \pm 0.06$). The errors assigned to D_2 are obtained from the spread of the slope values in the plateau region, thus they refer to the statistical errors in the data.

transformed into a chaotic attractor a noisy plateau at a value around 2 is visible.

V. NUMERICAL ANALYSIS

As discussed in the Introduction, our experiment is modeled by Eqs. (2). The first two equations describe the dynamics of a two-level homogeneously broadened class-B laser, with a loss constant depending on the delayed feedback variable z. The third equation describes the feedback loop as a low-pass filter. We focus on a region of the parameter space which is close to that investigated experimentally. The selected parameters for Eq. (2) are given in the caption of Fig. 8. We have performed a numerical integration of Eqs. (2), using a fourth-order Runge-Kutta method.

The results of this numerical analysis are based on the same indicators used for the experimental characterization, i.e., phase-space portraits, power spectra, and autocorrelation functions.

As shown in Fig. 8, increasing the bias parameter B we observe the transition from a steady-state behavior (not reported) to a periodic solution [Fig. 8(a)]. A further increase leads to the appearance of a second incommensurate frequency [Fig. 8(b)], whose amplitude becomes larger and larger [Fig. 8(c)]. We find also locking windows [Fig. 8(d)] and their subharmonic destabilization [Fig. 8(e)], up to a weakly chaotic behavior [Fig. 8(f)] with a slow decay rate of the autocorrelation function, such as reported in Fig. 3(e).

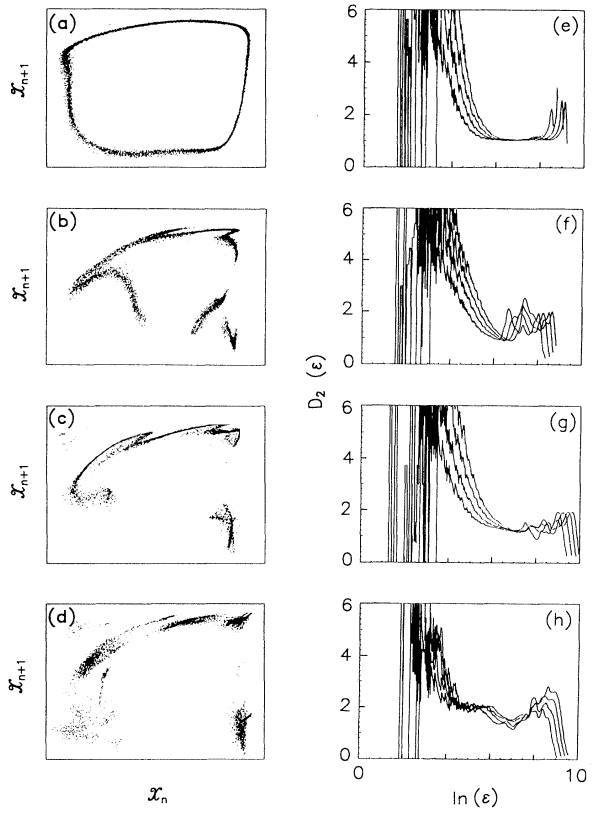

FIG. 7. Poincaré sections and associated correlation integral slopes at the torus breaking calculated on 10 000 points. (a) $B=660$ V; (b) $B=665$ V; (c) $B=667$ V; (d) $B=671$ V.

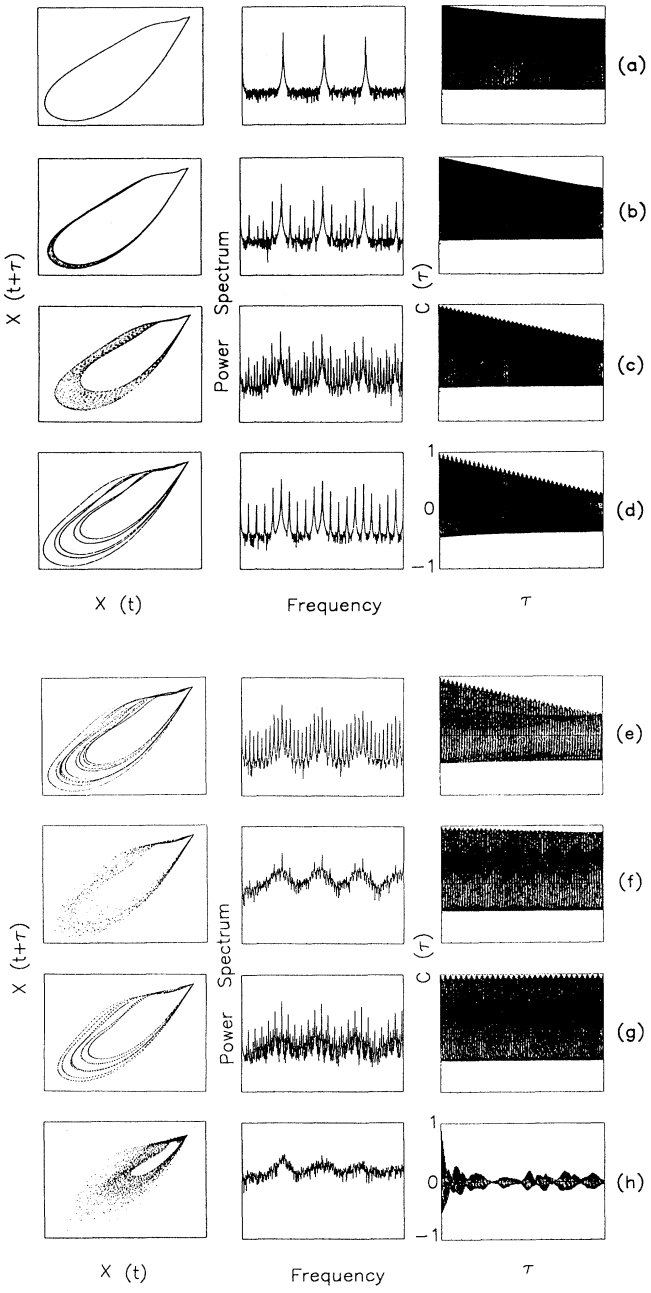

FIG. 8. Numerical results. Left column: phase-space portraits; central column: power spectra; right column: autocorrelation functions. Parameter values: $A=4.0$, $\alpha=0.2$, $r=0.6$, $\beta=4.0\times10^6$ s^{-1}, $k=2.0\times10^7$ s^{-1}, $\gamma=6.0\times10^4$ s^{-1}, $\tau=5$ μs. (a) $B=0.4$; (b) $B=0.46$; (c) $B=0.5$; (d) $B=0.63$; (e) $B=0.66$; (f) $B=0.68$; (g) $B=0.75$; (h) $B=0.8$. Here, B is normalized to $1/\pi$ times the half wavelength voltage of the modulator.

Increasing B again we find higher-order locking regions [Fig. 8(g)] and a fully developed chaotic behavior [Fig. 8(h)] with a fast decay rate of the autocorrelation function comparable to that of Fig. 3(g). The data reported in Fig. 8 show the qualitative agreement with the experiment. A complete numerical investigation would require a scanning of the two-dimensional parameter space (B,r) for fixed A, α, β, k, γ, and τ. In spite of this, we show how a linear stability analysis can lead to evaluation of the small amplitude oscillation frequencies starting from a steady-state solution of Eqs. (2). The steady-state nontrivial ($\bar{x}\neq 0$) solutions are given by the following equations:

$$A=(1+\bar{x})[1+\alpha\bar{x}(B-r\bar{x})]\,,$$
$$\bar{y}=A/(1+\bar{x})\,, \tag{7}$$
$$\bar{z}=B-r\bar{x}\,.$$

We specialize our calculations for $\alpha=0.2$, $B=0.4$, and $r=0.6$, parameters equal to those of the numerical simulations of Fig. 8, but $A=1.836$, which represents a close fit with the experimental situation. One of the three intensity solutions for the above numbers is $\bar{x}=0.877\,71$. We study the oscillatory solutions around this steady point. The linear stability analysis of the delayed system leads to an eigenvalue equation of transcendent type.[19] A similar analysis has been recently applied with reference to a semiconductor laser with delayed feedback.[20] In this case, it is straightforward to derive the following eigenvalue equation:

$$\left[\frac{s}{\beta}+1\right]\left[\frac{s}{k}\left[\frac{s}{\gamma}+1+\bar{x}\right]+\frac{A\bar{x}}{1+\bar{x}}\right]=r\alpha\bar{x}^2\left[\frac{s}{\gamma}+1+\overline{x}\right]e^{-s\tau}\,, \tag{8}$$

where $s=\lambda+i\omega$ is the complex eigenfrequency. The lowest-frequency solutions of this trascendent equation are plotted in Fig. 9. The corresponding real parts λ give the damping (if negative) or amplification factor (if positive). The solution denoted by an arrow has a positive real part hence it has to be related to the limit cycle of Fig. 8(a) (model) and Fig. 3(a) (experiment). The presence of adjacent frequencies with a relatively small damping rate show that a two-frequency behavior of toroidal type may appear.

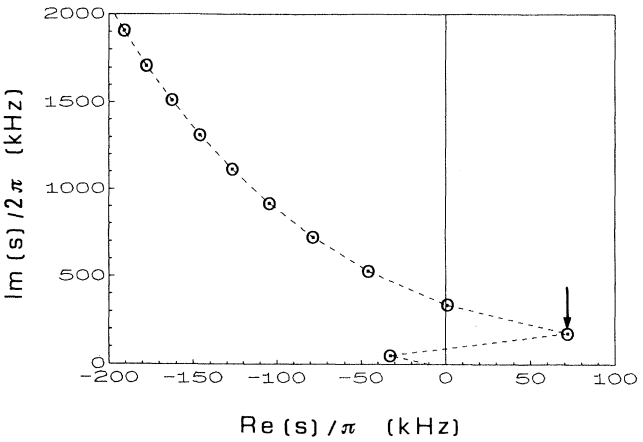

FIG. 9. Linear stability analysis at the fixed point $\bar{x}=0.877\,71$. The circled dots represent the poles of the Laplace transform of the linearized variables. The pole marked by the arrow corresponds to a frequency $f\simeq 176$ kHz.

VI. CONCLUSIONS

We have presented an experimental and theoretical study of the dynamics of a single-mode class-B laser with delayed feedback.

We have discussed also the analogy between our system and that of Ikeda, and shown under what conditions our problem can be reduced to the Ikeda one. We have presented a critical comparison between our results and the conjecture of Le Berre *et al.* on the fractal dimensions of Ikeda's chaotic attractor.

The wealth of experimental data here offered shows the peculiarities of the delayed system already in the short delay regime where the number of DOF's is reasonably small. Very different phenomena occur when that number is consistently higher (larger than ten), and we refer to a planned paper[7] for the corresponding phenomenology. As for the model, we have solved numerically the equations and given the steady-state solution and a linear stability analysis in a parameter range close to the experimental one. A qualitative agreement is achieved. A closer fitting of experiment and theory would require a lengthy detailed scanning of the parameter space.

ACKNOWLEDGMENTS

We are grateful to Dr. G. P. Puccioni for help in the data analysis.

*Also at: Department of Physics, University of Florence, Florence, Italy.

[1]P. Bergé, Y. Pomeau, and C. Vidal, *Order Within Chaos* (Wiley, New York, 1986); H. G. Schuster, *Deterministic Chaos* (VCH, New York, 1988). The pioneering experiments on low-dimensional chaos are collected in *Universality in Chaos*, edited by P. Cvitanovic (Hilger, London, 1989).

[2]H. Haken, Phys. Lett. **53A**, 77 (1975).

[3]F. T. Arecchi, in *Instability and Chaos in Quantum Optics*, edited by F. T. Arecchi and R. G. Harrison (Springer-Verlag, Berlin, 1987), pp. 9–48.

[4]F. T. Arecchi, W. Gadomski, and R. Meucci, Phys. Rev. A **34**, 1617 (1986); F. T. Arecchi, A. Lapucci, R. Meucci, and J. A. Roversi, Europhys. Lett. **6**, 677 (1988); F. T. Arecchi, W. Ga-

domski, A. Lapucci, H. Mancini, R. Meucci, and J. A. Roversi, J. Opt. Soc. Am. B **5**, 1153 (1988).
[5]J. D. Farmer, Physica **4D**, 366 (1982).
[6]J. Mallet-Paret, J. Differ. Equ. **22**, 331 (1976).
[7]F. T. Arecchi, G. Giacomelli, A. Lapucci, and R. Meucci (unpublished).
[8]F. T. Arecchi, G. Giacomelli, A. Lapucci, and R. Meucci, "Experimental Evidence of Quasiperiodicity Route to Chaos in a CO_2 Laser with Delayed Feedback," in Tech. Digest of Nonlinear Dynamics in Optical Systems, Afton, Oklahoma 4–8, June 1990.
[9]C. E. Shannon, Proc. Inst. Radio Eng. **37**, 10 (1949).
[10]B. Dorizzi, B. Grammaticos, M. Le Berre, Y. Pomeau, E. Ressayre, and A. Tallet, Phys. Rev. A **35**, 328 (1987).
[11]M. Le Berre, E. Ressayre, A. Tallet, H. M. Gibbs, D. L. Kaplan, and M. H. Rose, Phys. Rev. A **35**, 4020 (1987).
[12]K. Ikeda, Opt. Commun. **30**, 257 (1979); K. Ikeda, H. Daido, and O. Akimoto, Phys. Rev. Lett. **45**, 709 (1980); H. M. Gibbs, F. A. Hopf, D. L. Kaplan, and R. L. Shoemaker, Phys. Rev. Lett. **46**, 474 (1981); M. Okada and K. Takizawa, IEEE J. Quantum Electron. **QE17**, 2135 (1981); K. Ikeda and K. Matsumoto, Physica **29D**, 223 (1987).
[13]D. Ruelle and F. Takens, Commun. Math. Phys. **20**, 167 (1971); S. Newhouse, D. Ruelle, and F. Takens, Commun. Math. Phys. **64**, 35 (1978).
[14]M. Le Berre, E. Ressayre, and A. Tallet, Opt. Commun. **72**, 123 (1989).
[15]G. L. Oppo and A. Politi, Europhys. Lett. **1**, 544 (1986); Phys. Rev. A **40**, 1422 (1989).
[16]F. T. Arecchi, G. Giacomelli, A. Lapucci, and R. Meucci (unpublished).
[17]P. Grassberger and I. Procaccia, Phys. Rev. Lett. **50**, 346 (1983).
[18]R. Badii, G. Broggi, B. Derighetti, M. Ravani, S. Ciliberto, A. Politi, and M. A. Rubio, Phys. Rev. Lett. **60**, 979 (1988).
[19]N. Minorsky, in *Nonlinear Oscillations,* edited by D. Van Nostrand (Princeton University, Princeton, NJ, 1962).
[20]G. Giacomelli, M. Calzavara, and F. T. Arecchi, Opt. Commun. **74**, 97 (1989).